Automated Virtual Prototyping of Permanent Magnet Synchronous Machines for HEVs

Martin Hafner, Thomas Finken, Matthias Felden and Kay Hameyer
Institute of Electrical Machines – RWTH Aachen University
Schinkelstraße 4, D-52062 Aachen, Germany
E-mail: Martin.Hafner@IEM.RWTH-Aachen.de

***Abstract*—Hybrid electrical vehicles (HEV), which combine the drive power of an internal combustion engine and that of one or several electrical machines (EM), are finding, due to an increasing ecological awareness, a better market acceptance nowadays. Due to the limited space available in drive trains, PMSMs, which offer high power densities, are prime candidates for such applications. This paper presents an automated design process for PMSM, which reduces the development time and allows considering many design variations.**

I. Introduction

Electric and hybrid electric vehicles are the focus of an intense research activity nowadays. The contradictory requirements on the power train, such as high efficiency, high overload capacity and small installation space, make it so that many machine types are actually candidates for the electrified traction.

According to several comparative studies [1], [2], the permanent magnet synchronous machine (PMSM) appears to be best suited for such applications. In an earlier work by this author [3], a design and optimization procedure for an internal mounted PMSM (IPMSM) with fixed outer dimensions has been proposed, which determines the machines characteristics by different finite element (FE) simulations and corresponding post-processing routines. Since IPMSMs exhibit a strongly non-linear flux-current characteristic, all quantities such as induced voltage, synchronous and reluctance torque, optimal field weakening angle and inductances have to be computed explicitly at each considered operation point. This requires numerous 2D transient FE computations, leading to a high computational time and an additional time-consuming evaluation effort for the design engineer.

Therefore, all proposed routines and evaluation methods are combined into an automated tool chain, that allows computing all machine characteristics of several design candidates. This method can efficiently be parallelized, so that, if enough computer resources are available, in minimum four times of the computation time of one FE simulation is necessary. This allows increasing the number of parameters in the design and optimization process of an IPMSM by significantly decreasing the development time.

II. Numerical Methods for an Automated Machine Computation

Since PMSMs exhibit (especially in case of rotors with buried magnets) a strongly nonlinear behavior, the design process has to consider saturation- and flux-leakage effects, which cannot be determined accurately by analytical formula, and quasi-static numerical FE simulations need to be performed for each geometry. Fig. 1 shows a flowchart describing an automated process for the calculation of all relevant machine characteristics. In the following, the function of each operational block in the chart is described. All simulations were conducted with the in-house FEM software package iMOOSE [4].

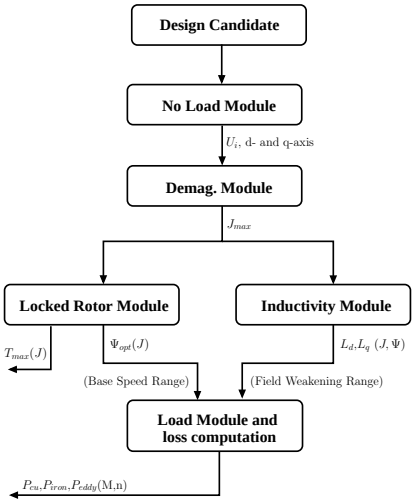

Fig. 1. Flowchart of the automated design process for a PMSM.

Initially, a ***No-Load Simulation*** is performed to calculate the stator phase flux-linkages and its time derivative, the back-emf, as well as to evaluate the occurring frequency higher harmonics. On basis of the motors maximal speed and DC link voltage U_{DC}, the designer can identify the best winding configuration. Moreover, this computation step detects the position of the d- and q-axis for further processing steps.

The electromagnetic overload capability of PM motors is limited by the demagnetization strength of the permanent magnet material. To determine the specific overload capability of a given design candidate, a ***Demagnetization Test*** is conducted. In worst case, e.g. by a fault in the power electronics and control, the maximum current is fed into negative direct axis ($I_d = -I_{max}$) weakening the flux density inside the permanent magnets according to its demagnetization curve. The level of demagnetization should not lead to an irreversible demagnetization. In order to determine this physical limit, a current is fed in negative direct axis whose magnitude is stepwise increased so as to determine the maximum current I_{max}, still having a working point on the linear part of the demagnetization characteristic. Fig. 2 shows the minimal flux density within the magnets as a function of the current density varying the thickness of the PM material.

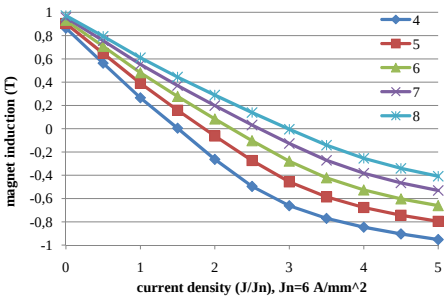

Fig. 2. Exemplary result of a demagnetization test for several magnet heights.

The torque of an IPMSM ($X_q > X_d$) is given by:

$$T = \frac{3p}{\omega} \cdot [U_p - I_d \cdot (X_q - X_d)] \cdot I_q, \tag{1}$$

where p is the pole pair number, ω the angular frequency and U_p the back-emf. It consists of the synchronous torque T_{syn} and the reluctance torque T_{rel}:

$$T = \underbrace{\frac{3p}{\omega} \cdot U_p I_q}_{T_{syn}} - \underbrace{\frac{3p}{\omega} \cdot I_q I_d \cdot (X_q - X_d)}_{T_{rel}}. \tag{2}$$

Inserting $I_q = I\cos\psi$, $I_d = I\sin\psi$, where ψ is the field-weakening angle, the torque can be rewritten as:

$$T = \hat{T}_{syn}\cos(\psi) - \hat{T}_{rel}\sin(2\psi) \tag{3}$$

i.e. the sum of a fundamental ($\hat{T}_{syn}$) and the first harmonic ($\hat{T}_{rel}$) which are constant for a given current. The phase voltage U_s, see Fig. 3, is given by

$$U_s = U_p + \jmath X_q I_q + \jmath X_d I_d + R_1 (I_q + I_d), \tag{4}$$

where R_1 is the phase resistance. For operation points in

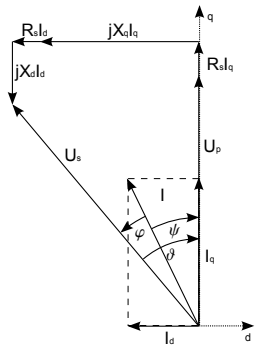

Fig. 3. The phasor diagram of a synchronous machine with saliency.

the base speed range (Region 1) the phase voltage U_s is below the maximum voltage, which in turn is limited by the dc-link voltage of the power converter, so that the phase current is constrained by the magnet demagnetization and further thermal limitations or the power electronic's maximal current. Differentiating (3) with respect to ψ, one sees that the maximum torque T_{max} per current (MTPA-control) is realized for the so called optimal field-weakening angle ψ_{opt}, cf. Fig. 4. The ***"Locked-Rotor Test"*** is thus made to determine the absolute values of the synchronous torque $\hat{T}_{syn}$ and the

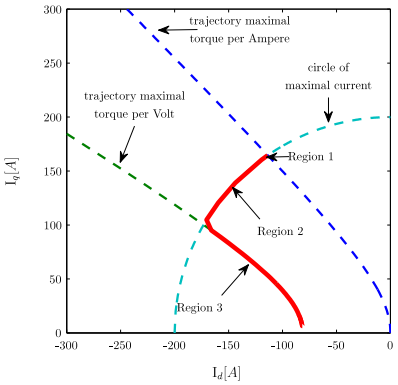

Fig. 4. PMSM operation points in the I_d-I_q coordinate system.

reluctance torque $\hat{T}_{rel}$, as well as to determine the optimal field-weakening angle ψ_{opt} and the maximum torque T_{max}. This calculation is performed for a stepwise increasing stator-current density in order to capture the dependency of those quantities on the load current as exemplified in Fig. 5.

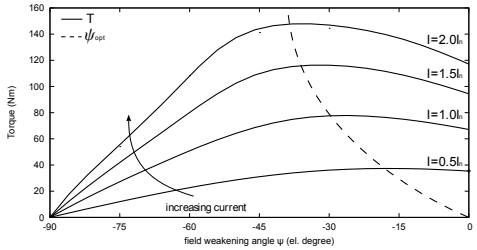

Fig. 5. The average torque over ψ, resulting from the "locked-rotor test".

For operation points in the field weakening range, the control strategy of the power converter limits the phase voltage to its maximum by shifting ψ according to Fig. 3. For the simulation of this control strategy (Region 2, in Fig. 4), the direct- and quadrature-axis inductances (L_d and L_q), which are both function of the load current and the field weakening angle ψ, are calculated by means of the L_dL_q***-Computation***, see Fig. 6. By knowing the inductances L_d and L_q and

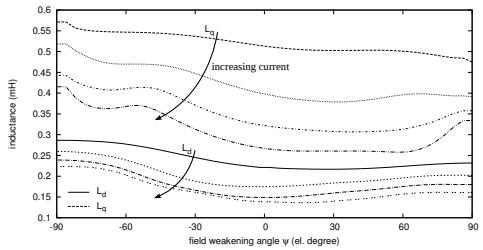

Fig. 6. Exemplary result of a inductance computation in function of the field weakening angle ψ and the current.

a corresponding field weakening angle the electromagnetic torque for each operation point is given by (1). In some cases, according to the quantities L_d and L_q, there exists a operation point within the field weakening range, where a further increase of the rotor speed n requires to reduce the current below its maximum. From here on (Region 3, in

Fig. 4), the power controller follows the maximum torque per voltage curve (MTPV-control).

In order to evaluate and rate the motor's energy consumption and efficiency, all losses need to be determined for all operation points. This computation is conducted by the ***Operation Point Simulation***. At this step, the optimal field-weakening angle ψ_{opt} is used to set the maximum torque in base speed range, whereas ψ has to be set by means of control strategies in the field weakening range. Ohmic losses P_{cu} are estimated taking end windings into account. Iron losses are computed by means of quasi-static numerical FE simulations and an improved post-processing formula based on the loss-separation principle [5], [6] considering rotational hysteresis losses as well. The implemented formula assumes a separability of the iron losses (P_{Fe}) into hysteresis losses (P_h), eddy-current losses (P_{ec}) and excess losses (P_{ex})

$$P_{Fe} = P_h + P_{ec} + P_{ex}, \tag{5}$$

where P_{ec} and P_{ex} are computed from the contributions of each harmonic of the flux density over one electrical period, whereas P_h is determined as a function of the peak value of the magnetic-flux density on the same time interval. The eddy-current density in the permanent magnets is calculated by means of a transient 3D-FE approach, as described in [7]. The eddy-current density J_{ec} and the specific conductivity of the magnet material σ_{pm} are used to determine the eddy-current losses P_{eddy} by integration over the magnet's volume V_{pm}:

$$P_{eddy} = \int \frac{1}{\sigma_{pm}} \vec{J}_{ec}^{\,2} dV_{pm} \tag{6}$$

By performing the loss calculation it is possible to determine the total losses P_{tot} for each operation point given by:

$$P_{tot} = P_{cu} + P_{Fe} + P_{eddy} + P_{mech}, \tag{7}$$

where P_{mech} are the mechanical losses depending on bearing and fan configurations - P_{mech} is neglected in this paper. In the machine's overall energy balance, the loss terms P_{Fe} and P_{eddy} are counteracting the electromagnetic torque T_{el}, because both energy terms are neglected in the electromagnetic FE governing equation, so that the measurable active torque can be expresses as:

$$T_{act} = T_{el}\left(n, J, \psi\right) - \frac{P_{Fe}\left(n, J, \psi\right) + P_{eddy}\left(n, J, \psi\right)}{2\pi n}. \tag{8}$$

Resulting from the total losses and the input power P_{in},

$$P_{in} = 2\pi n \cdot T_{el}\left(n, J, \psi\right) + P_{cu}\left(J\right), \tag{9}$$

the efficiency η can be calculated in function of speed and torque:

$$\eta = \frac{2\pi n \cdot T_{act}\left(n, J, \psi\right)}{P_{in}\left(n, J, \psi\right)}. \tag{10}$$

Afterwards the results can be visualized as two-dimensional color maps, e.g. efficiency maps, as exemplary given in Fig. 7. In order to generate such a map, the Region 1 in Fig. 4 is discretized by N^1_{Map} operation points, whereas Region 2 and 3 are sampled by N^2_{Map} points.

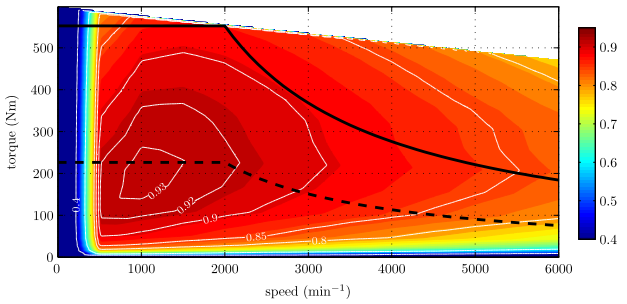

Fig. 7. Exemplary result of the efficiency of a PMSM according to (8)-(10).

III. The Aspect of Parallelization

The primary requirement of the development process for electrical machines (EM) in hybrid electrical vehicles (HEV) is to simulate each design candidate over its whole torque-speed characteristic. This is crucial, since an evaluation of the drive's mean lifetime or average efficiency is based on a driving cycle analysis, i.e. a stochastic distribution of operation points, [8], [9], [10]. The proposed design process, Fig. 1, is capable of this by computing the nonlinear machine characteristic, as well as the T-n diagram by numerous 2D transient, quasi-static FE computations. In consequence, the determination on the overall machine behavior requires a high computational effort. This leads, in case of a sequential processing, to a long simulation time. To limit and minimize this time delay in the design procedure, the necessary FE simulation, described in section II, can be processed in parallel. Reorganizing the flowchart of Fig .1 into a time-line diagram, given in Fig 8, shows that the response time can be shorten to a minimal duration of four FE simulations. Since the computational blocks, such as ***No-Load***

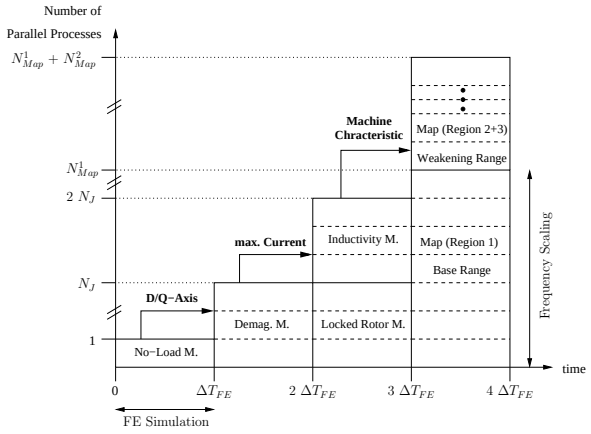

Fig. 8. Parallelization of the automated design process as line-line diagram, showing the necessary number of parallel processes in function of time.

Simulation and ***Demagnetization Test*** are interdependent, the load is unbalanced growing with each time-step (ΔT_{Fe}), where all modules to identify the machine characteristics are carried out by a current discretization of N_J. According to (1) a variation of the rotor speed n does not effect the quantities I_d, I_q and thus the variables J, ψ of the MTPA-control. Therefore, in case of base speed range, the discretization of the rotor speed (n-axis) in the efficiency maps can be replaced

by rescaling (5) for a specific frequency f to an arbitrary frequency $\tilde{f}$ by

$$P_{Fe}\left(\tilde{f}\right) = P_h\left(f\right)\cdot c + P_{ec}\left(f\right)\cdot c^2 + P_{ex}\left(f\right)\cdot c^{1.5}, \quad (11)$$

where $c = \tilde{f}/f$. By this, the behavior in base speed range can be computed by N^1_{Map} current variations. Such a simplification is not applicable in Region 2 and 3 (MTPV-control), where the operation points need N^2_{Map} additional computations to be calculated explicitly. Therefore, N^2_{Map} is quite larger than N^1_{Map}. The described automation process is integrated in the in-house software package ProMOTOR [11] which also manages the cluster computing.

IV. FE-Added Design Example

The automated virtual prototyping described in section II and III has been applied in [3], [10] to design a 30 kW IPMSM for a full HEV application under a total length limitation of 160 mm and a volume restriction to 9.2 dm^3. In case of a development with limited available installation space and fixed outer dimensions, the primary sizing parameters are the rotor radius R_r and the pole pair number p. For a given phase current density up to J_{max} (which depends in particular on the type of cooling considered), R_r has an optimum with respect to the maximal torque T and output power P, since an increase of R_r decreases the effective winding area (stator flux) but positively impacts the rotor flux per pole. Increasing the number of poles p implies decreasing the magnet width and enlarging the relative amount of magnet leakage flux, which in turn reduces the air gap flux density and therefore the maximum of T. The evaluation of the R_r-p parameter space for concentrated (CW) and distributed (DW) winding configurations is performed initially as a predesign step by the ***"Locked-Rotor Test"***, as shown in Fig. 9, in order to determine the best R_r-p combinations. Parameters in the second step

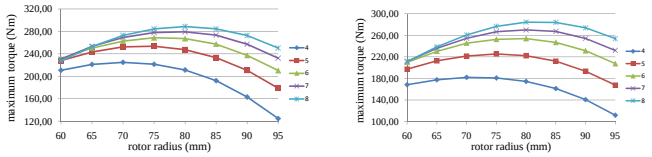

(a) CW, $I = I_n$ (b) DW (q=2), $I = I_n$

Fig. 9. The maximal torque in function the pole pair number p and the rotor radius R_r for a concentrated (CW) and distributed (DW) winding configuration.

of the design that affect the overload capability, determined by ***Demagnetization Test***, are the magnet height m_h and the pole pitch factor τ_p. Since the computation and evaluation process are autonomous, the preliminary design study can consider a high number of parameter combinations (about 100 within this project). The best suited design candidates, are afterwards analyzed in detail over the whole operation range with respect to the motor efficiency, Fig 7. Therefore, these maps characterizing the machine's efficiency are fed into a vehicle-simulation model [12], which contains the vehicle data, the transmission, the battery, the battery controller and the main vehicle control unit.

V. Conclusion

In contrast to classical design approaches for PMSMs, requiring a specific torque and speed in one, sometimes in a few points, the main requirement for those drives in HEV applications is a high overall efficiency within a large range of the torque-speed characteristic, a high overload capacity and small installation space and weight.

This paper presents a formalism to design, evaluate and optimize the PMSM drive for its individual application purpose. The associated analysis is carried out as an flowchart based automated design process. To minimize the allover simulation response time, the aspect of parallelization is considered as well, allowing to schedule the analysis on a computer cluster. This allows to consider a large number of degrees-of-freedom, e.g. a wide design parameter space, to find the optimal parameter combination under given constraint for an individual application in short time. The proposed method already contributes in industrial projects and can be applied generally in the design of permanent magnet synchronous machine.

References

[1] M. Zeraoulia, M. Benbouzid, and D. Diallo, "Electric motor drive selection issues for HEV propulsion systems: A comparative study," *IEEE Transactions on Vehicular Technology*, vol. 55, no. 6, pp. 1756–1764, 2006.

[2] T. Finken, M. Felden, and K. Hameyer, "Comparison and design of different electrical machine types regarding their applicability in hybrid electrical vehicles," in *18th International Conference on Electrical Machines, ICEM*, 2008, pp. 1–5.

[3] T. Finken and K. Hameyer, "Design and optimization of an IPMSM with fixed outer dimensions for application in HEVs," in *IEEE International Conference on Electric Machines and Drives, IEMDC*, 2009, pp. 1743–1748.

[4] D. van Riesen, C. Monzel, C. Kaehler, C. Schlensok, and G. Henneberger, "iMOOSE-an open-source environment for finite-element calculations," *Magnetics, IEEE Transactions on*, vol. 40, no. 2, pp. 1390–1393, 2004.

[5] G. Bertotti, A. Boglietti, M. Chiampi, D. Chiarabaglio, F. Fiorillo, and M. Lazzari, "An improved estimation of iron losses in rotating electrical machines," *Magnetics, IEEE Transactions on*, vol. 27, no. 6, pp. 5007–5009, 1991.

[6] M. H. Gracia, E. Lange, and K. Hameyer, "Numerical calculation of iron losses in electrical machines with a modified Post-Processing formula," in *16th International Conference on the Computation of Electromagnetic Fields, COMPUMAG*, Aachen, Germany, 2007.

[7] C. Kaehler and G. Henneberger, "Eddy-current computation in the claws of a synchronous claw-pole alternator in generator mode," *Magnetics, IEEE Transactions on*, vol. 38, no. 2, pp. 1201 –1204, Mar. 2002.

[8] D. Bucher, R. Nuscheler, W. Meyer, and H. Herzog, "Comparison of electrical machine types in hybrid drive trains: Induction machine vs. permanent magnet synchronous machine," in *18th International Conference on Electrical Machines, ICEM*, 2008, pp. 1–6.

[9] H. Neudorfer, N. Wicker, and A. Binder, "Comparison of three different electric powertrains for the use in hybrid electric vehicles," in *4th IET Conference on Power Electronics, Machines and Drives, 2008. PEMD 2008.*, 2008, pp. 510 –514.

[10] T. Finken, M. Hafner, M. Felden, and K. Hameyer, "Design rules for energy efficient IPM motors in HEV applications," in *International Conference and Exhibition on Ecological Vehicles and Renewable Energies, EVER*, Monaco, Mar. 2010.

[11] M. Schoning and K. Hameyer, "Virtual product development for electrical motors," in *IEEE International Conference on Electric Machines and Drives, IEMDC*, vol. 2, 2007, pp. 949–952.

[12] T. Markel, A. Brooker, T. Hendricks, V. Johnson, K. Kelly, B. Kramer, M. O'Keefe, S. Sprik, and K. Wipke, "ADVISOR: a systems analysis tool for advanced vehicle modeling," *Journal of Power Sources*, vol. 110, no. 2, pp. 255 – 266, 2002.